PERGAMON

International Journal of Heat and Mass Transfer 45 (2002) 1535–1543

International Journal of HEAT and MASS TRANSFER

www.elsevier.com/locate/ijhmt

Experimental and theoretical study of axial dryout point for evaporation from V-shaped microgrooves

Sivaraman Anand, Sirshendu De, Sunando Dasgupta *

Department of Chemical Engineering, Indian Institute of Technology, Kharagpur, PIN 721 302, India

Received 27 July 1999

Abstract

Experiments are carried out in a specially designed cell to study the onset and propagation of dryout point on a chemically machined microgrooved silicon surface with pentane as the coolant liquid. The axial temperature distribution is accurately measured as a function of the heat input and inclination of the substrate. The comparison between the dry (without liquid) and wet (with liquid) temperature profiles is used to locate the dryout point. The axial flow of an evaporating thin liquid film through a V-shaped microgroove with an appreciable inclination angle and varying evaporative heat flux is theoretically investigated. The nonlinear governing equations are solved numerically to predict the onset, location and propagation of the dryout point. The predictions from the theoretical analysis are successfully compared with the experimental results.

1. Introduction

Microscale heat exchange is currently an active area of research due to its possible applications in several technologically important processes, e.g. in the electronic packaging industry, cooling of solar panels in microgravity environments, and spacecraft thermal control. The current concepts in integrated circuits packaging are motivated by the development of MOS and VLSI technologies, requiring higher levels of device integration. The increases in the required power dissipation will result in increased thermal gradients and higher mean operating temperatures of the device. Thus it is necessary to develop new types of thermal control schemes capable of removing heat from the chip and reduce the mean-time-between-failure of these devices. In cases where large amounts of heat must be removed, the use of change of phase heat transfer mechanism can prove to be a promising choice. This technique has been widely used in various cooling operations, through the utilization of heat pipes for the thermal control of electronic components.

In 1984, Cotter first proposed the concept of microheat pipe [1], which essentially is a wickless heat pipe for the uniform temperature distribution in electronic chips. In practical terms a microheat pipe is a wickless, non-circular channel with a diameter of 10–500 μm and a length of 10–20 mm. The flow of fluids inside the pipe is caused by the change in pressure (due to capillary and intermolecular force field change) along the length of the pipe. The net capillary force is generated by the integral effect of the evaporating and condensing menisci [2]. In order to design and optimize these cooling devices, it is necessary to understand and analyze the phenomena that control the behavior of the various interfaces, particularly the liquid–vapor interface which is primarily governed by the surface tension forces, wettability and the solid–liquid interactions. The pioneering works of Derjaguin and his co-workers developed the foundation for studying the interfacial transport processes in thin films. Derjaguin evaluated the excess potential present in the thin film of liquid because of the intermolecular forces of attraction and repulsion using the Dzyaloshinskii–Pitaevskii (DLP) theory and expressed it in terms of disjoining pressure [3]. Using adsorption isotherms and the disjoining pressure concept, it was demonstrated that thin film transport is capable of enhancing evaporation from

* Corresponding author.

0017-9310/02/$ - see front matter
PII: S0017-9310(01)00245-9

Nomenclature

c_3	constant dependent on groove geometry [22]
g	acceleration due to gravity (m/s^2)
Gr	Grashof number
h_{fg}	latent heat of vaporization (J/kg)
K	constant in expression for c_3 (characteristic value of 13.33 for pentane)
L	length of channel (m)
P	total pressure (N/m^2)
p_c	capillary pressure (N/m^2)
q_b	total input heat flux (J/m^2)
$q''(x)$	heat flux normal to the bottom of the plate (J/m^2)
$Q''(X)$	non-dimensionalized heat flux normal to the bottom of the plate
$r(x)$	radius of curvature (m)
$R(X)$	non-dimensionalized radius of curvature
Re	Reynolds number
T	temperature (°C)
ω	half of the top groove width (m)
ω_b	groove pitch (m)
x	coordinate along the groove channel in the evaporative region
x'	coordinate along the groove channel in the adiabatic region
X	dimensionless length in the evaporative region
X'	dimensionless length in the adiabatic region

Greek symbols

α	half the vertex angle of the groove
β	inclination of the substrate
Γ_v	mass flow rate per unit area in the x-direction (kg/m^2 s)
v	kinematic viscosity (m^2/s)
ρ	density (kg/m^3)
σ	surface tension of the liquid (N/m)

Subscripts

a	adiabatic
amb	ambient
cap	capillary
conv	convection
e	evaporator
g	gas
j	junction of the intrinsic meniscus and the interline region
l	liquid
max	maximum length of meniscus along the axial or groove side direction
ref	ambient/reference
v	vapor

capillaries [4]. The spontaneous redistribution of fluid along an interior corner of a container due to capillary forces in the low-gravity environment of space under isothermal conditions was studied in detail by Weislodel and Lichter [5]. The models of stable evaporating meniscus were based on the hypothesis that the fluid flow in the evaporating meniscus resulted from a change in the meniscus profile, which created the necessary pressure gradient and demonstrated the importance of the various regions of a thin film during evaporative heat transfer [6–11].

Important contribution to the related area of heat transfer from small devices was made by Peterson and his co-workers. Babin et al. [12] tested a trapezoidal heat pipe with a square cross-section of 1 mm^2 and a length of 57 mm. Wu and Peterson [13] studied a wickless microheat pipe of dimension $1 \times 1 \times 10$–100 mm^3. They successfully used the Young–Laplace equation to describe the internal fluid dynamics of this integrated device. From these works it had been concluded that the longitudinal groove design was crucial to increase the heat transport capacity of these miniature devices and the small grooves provided the necessary capillary forces for the liquid to flow back into the evaporative zone. An analytical model [14] was developed to predict the heat transfer characteristics of the film evaporating from a V-shaped microgroove and compared it with the experimental data. The minimum meniscus radius and maximum heat transport in triangular grooves were also studied [15]. In recent years, many researchers have investigated the concept of using microheat pipes as effective heat spreaders [16] and into the concept of dryout point [17] and the apparent variation of its position along the length of the channel. Though valid for small tilt angles, the work provided useful information on the design restrictions and utility of microheat pipes.

The objective of the present work is to experimentally validate the onset of the dryout and its propagation along the length of the channel, as a function of system parameters, for large tilt angles. The position of the dryout point can provide us with useful information on the design and operating range of microheat pipes. A numerical solution scheme is adopted and the analyses are also not restricted to the case of a constant heat flux in the evaporator regions as was used in [17]. The experimentally obtained temperature profiles are analyzed to evaluate the evaporative heat flux as a function of position which in turn is used in the numerical solution of the model and the prediction of the occurrence and position of the dryout point is compared with the experimental observations.

2. Experimental study

The experiments are performed on a specially designed cell. The V-shaped microgrooves are etched on the silicon wafer using chemical machining method, and a computer controlled mechanical surface profilometer is used to verify their apex angles and dimensions. The cell is equipped with a standard heat source, providing stable measurable power to the hot end, mimicking the hot spots on electronic chips. The axial temperature profiles on the microgrooved silicon substrate are measured, with and without the working liquid (coolant), using small thermocouples (each individually calibrated with an accuracy of ±0.1 °C). Each experiment (for each power input and inclination) is repeated three times. All the experiments show a repeatability to within ±3% in terms of the temperature measurements for the different runs. The largest differences that are observed at the first thermocouple (nearest to the heater) yet are always less than ±6% and are probably due to the small discrepancies of placing the heater at the exact position. The results are compared with the temperature profiles of a non-grooved substrate. The comparison of the profiles, dry (without coolant) and wet (with coolant), is used to verify whether the dryout point has been reached, as detailed in Section 3. The experiments are carried out using pentane as the working fluid.

The experimental test facility illustrated in Figs. 1 and 2 consists of V-shaped microchannels, etched on a silicon wafer and partially immersed in a pool of liquid coolant. The length of each channel (L) is equal to 2.5 cm. The liquid is kept in place inside the leakproof aluminum chamber with the help of O-rings. The wafer is inclined to the horizontal and constant heat flux is supplied to one end (upper) of the channel. The liquid wicks up the grooves by capillary action, against the gravitational force and the frictional pressure drop, resulting in a continuous flow of fluid towards the hot spot. The parameters affecting the evaporation process are the heat input, channel geometry (channel length, groove angle, channel width), the angle of inclination, thermophysical properties of the coolant liquid, and the nature of the substrate. The choice of a specific liquid

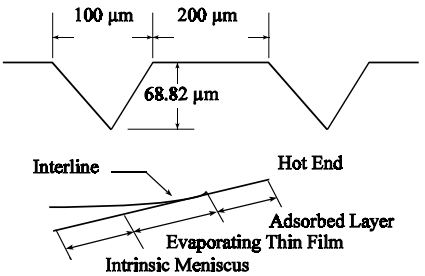

Fig. 1. Groove geometry and the description of the meniscus.

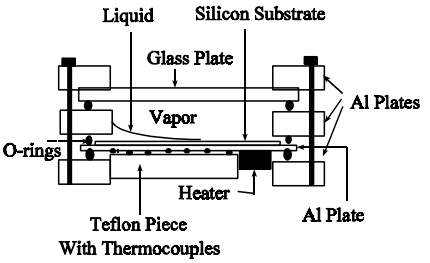

Fig. 2. Schematic diagram of the experimental set-up.

should depend, among other things (e.g. wettability), on the operating temperature range.

The silicon substrate (0.8 cm × 2.8 cm) is bonded on a thin aluminum plate, so that the stress due to the tightening of the bolts is absorbed by the aluminum plate rather than the brittle and already weakened (due to the etching of the grooves) silicon substrate. Such an arrangement ensures that there is absolutely no vapor loss from the experimental chamber. A resistance heater and small thermocouples are attached to the back surface of the substrate. The resistance heater is held in place by a Teflon base that keeps the heater pressed against the substrate assembly. The thermocouples are kept in contact with the heated substrate (at regular distances of about 1.5 mm) using a specially made Teflon holder. The substrate was enclosed in an aluminum chamber by O-rings to completely isolate it from the environment. The top part of the cell has a glass window through which the evaporating meniscus can be viewed.

The bottom aluminum plate has a rectangular opening, through which the connections for the thermocouple and heater are made. A liquid entry port is made in the middle aluminum plate, near the center, which allows charging of the working fluid (coolant), at the beginning of the wet runs. A specially fabricated stand and base plate arrangement is used to keep the substrate inclined at any tilt angle. The constant controlled power supply is obtained from an accurate stabilized DC regulated power supply unit. The thermocouples for temperature measurement are fabricated using copper–constantan and are individually calibrated. The thermocouples are routed through a channel selector to a microvoltameter which accurately measures the emf developed.

Prior to the start of the experiment, the cell parts are thoroughly cleaned by immersing them in absolute alcohol for half-an-hour. The components are further washed in acetone and the cleaned parts are placed in an oven for 45 min. The silicon wafer is cleaned separately with alcohol, followed by acetone. A final dip in buffered HF at 30 °C is used to remove oxides of silicon from the substrate surface. The cleaning and assembly of the experimental cell is performed in a class 100 clean hood to

prevent recontamination. A time period of at least 2 h is allowed between readings to ensure the attainment of steady state.

3. Experimental results and discussion

Experiments are conducted to evaluate the heat spreading capabilities of the grooved surface utilizing the change of phase heat transfer and to chart the propagation of the dryout point along the length of the channel, with changes in input power and inclination of the substrate. To evaluate the heat spreading enhancement, temperature profiles are plotted against the axial distance from the heater. By plotting $T - T_{ref}$, the driving force for heat transfer (T_{ref} being the prevailing ambient temperature) against position, the effect of any small perturbations in ambient temperature is minimized. Fig. 3 is indicative of the relative cooling effect of the grooved wafer with respect to the non-grooved wafer. As can be seen, substantial cooling has been achieved through use of the grooved wafer.

The onset of drying and its propagation away from the heater are presented in Figs. 4–6. It has been postulated that since there is no vapor loss from the system and the same amount of input power is used in both the wet and dry (no coolant used) runs, the two temperature profiles will be almost identical for the region near the heater from which the liquid has completely receded (dryout). This can be seen very clearly for the case of heat input of 1.52 W and for inclinations of 14.93°, 21.64° and 26.56°. Fig. 3 is for 0° inclination and there is substantial cooling effect, marked by the separation between the dry and wet temperature profiles. As the inclination angle and hence the opposing body force is increased (Figs. 4 and 5) keeping the power input and amount of liquid constant, the top portion (near the

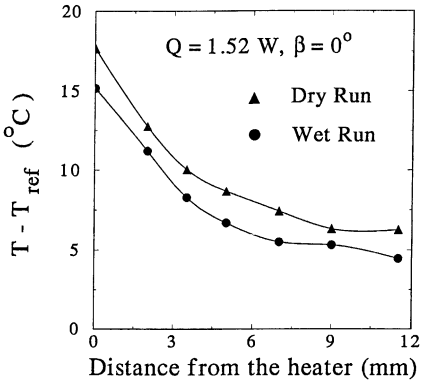

Fig. 3. Cooling achieved for a microgrooved surface with pentane as the coolant. Q (heat input) = 1.52 W, β (inclination) = 0°, T_{ref} (reference ambient temperature) = 35 °C.

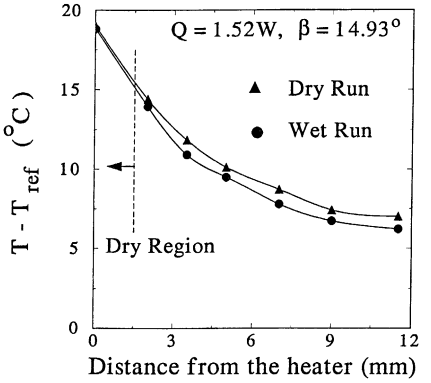

Fig. 4. Onset of dryout point. Q (heat input) = 1.52 W, β (inclination) = 14.93°, T_{ref} (reference ambient temperature) = 32.6 °C.

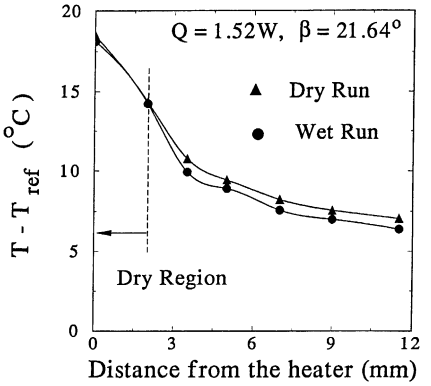

Fig. 5. Onset and propagation of dryout point. Q (heat input) = 1.52 W, β (inclination) = 21.64°, T_{ref} (reference ambient temperature) = 35.0 °C.

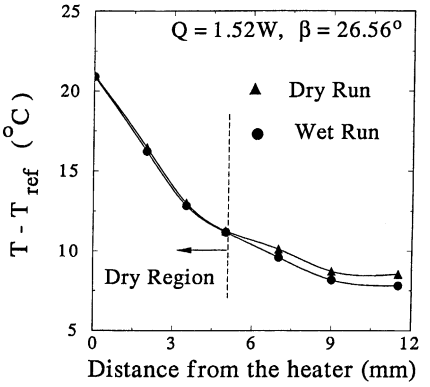

Fig. 6. Onset and propagation of dryout point. Q (heat input) = 1.52 W, β (inclination) = 26.56°, T_{ref} (reference ambient temperature) = 35.0 °C.

Table 1
Comparison between the experimental and theoretical locations of the dryout point (X_{max} is the distance from the hot end)

Power (W)	Inclination (°)	X_{max} (mm)		T_{amb} (°C)
		Theoretical	Experimental	
1.52	14.93	7.80	6.50	32.6
	21.64	8.20	7.50	35.0
	26.56	11.80	10.00	35.0
	38.66	13.60	12.50	33.0
	43.16	13.80	14.20	35.0
1.71	38.66	16.20	16.50	32.6
	90.00	16.40	16.50	32.6

heater) of the two profiles nearly overlaps (up to the second thermocouple for an inclination of 21.64°), emphasizing that dryout has been reached in this region. A further increase in inclination (Fig. 6) illustrates the further propagation of the dryout region, away from the heater towards the bulk liquid pool. A series of such runs at different power inputs generate a data set of dry out point locations as a function of power inputs and angles of inclination. A summary of such experimental results is presented in Table 1. It is to be noted that the ambient temperature plays a critical role in the evaluation of the origin and propagation of the dryout point. The effect of the varying ambient temperature is illustrated in Table 1, wherein the position of the dryout point for different inclinations of the substrate has been listed along with the prevailing ambient temperature. The variation in the maximum temperature reached for differing ambient temperatures can be noted in Figs. 4–6.

4. Theoretical formulation

The axial flow of an evaporating thin film through a V-shaped microchannel is investigated for the case of an inclined groove plate. The highest heat transfer coefficients typically occur when a pure substance or mixture undergoes a phase change. In cases, where this phase change involving evaporating or condensing fluids, small capillary grooves are often used to increase the effective liquid–vapor interfacial area for evaporation or the effective solid–vapor surface area for condensation. Using the technique of microgrooves, the size and thickness of the thin film region, the location and magnitude of the interline region, and the average heat transfer coefficient can all be significantly enhanced by controlling the number, cross-sectional shape and the length of the capillary grooves.

As illustrated in Fig. 1, when a liquid contacts a flat surface, the extended meniscus is divided into three regions, namely:

1. the intrinsic meniscus region, dominated by the capillary forces;
2. the evaporating thin film region where the combined effects of both capillarity and disjoining pressure are present;
3. the adsorbed layer region where disjoining forces dominate thereby inhibiting evaporation.

The current investigation modifies the general model developed by Ha and Peterson [17] by incorporating the variation of the evaporative heat flux with position along the length of the groove, which is a more realistic situation. Moreover, for the sake of completeness, the heat losses through convection from the top, bottom and sides of the substrate have also been taken into account while calculating the evaporative heat flux from any section of the substrate. A number of analytical models are available in the literature [7,10,11,18–21]. Though all these models are extremely important in understanding the evaporating flow up the groove wall, some of them are not directly applicable to small grooves. In order to better understand the transport processes of fluids in capillary grooves, the axial and cross-sectional flow characteristics occurring in the intrinsic meniscus must be investigated.

At a given cross-section the liquid film is adsorbed at the groove wall, forming an extended thin film region above the intrinsic meniscus. The distribution of the thin film on the groove wall induces a large pressure gradient in the liquid. In this region, dispersion forces dominate the film behavior. Since the resistance to flow in the evaporating thin film and adsorbed layer regions of the extended thin film is much larger than it is in the intrinsic meniscus region, the majority of axial flows are limited to the intrinsic meniscus region. Based on the above discussion, the following simplifying assumptions can be made to determine the axial dryout point. These are as follows:

1. The axial flow along the groove in the x-direction occurs primarily in the intrinsic meniscus region.
2. The radius of curvature of the intrinsic meniscus is a constant at any x, but the radius of curvature varies

axially along the groove, and the capillary pressure gradient due to this decreasing radius drives the fluid flow in the x-direction.
3. The disjoining pressure gradient due to the variation of the film thickness along the z-direction drives the film flow up the groove wall.
4. Evaporation occurs primarily in the thin film region, particularly near the interline.
5. The vapor pressure is constant.

The liquid–vapor interfacial pressure difference can be expressed by the Young–Laplace equation

$$p_v - p_l = \frac{\sigma}{r}, \tag{1}$$

where 'r' is the mean radius of curvature given by

$$\frac{1}{r} = \frac{1}{r_1} + \frac{1}{r_2}. \tag{2}$$

At each point on the liquid–vapor interface, the surface has two principal radii of curvature, r_1 and r_2, in orthogonal planes normal to the surface. One of the radii, the axial radius, r_2, approaches infinity when compared to the other comparatively smaller radius, r_1, of the intrinsic meniscus. Hence the mean effective curvature can be expressed as

$$\frac{1}{r} \cong \frac{1}{r_1}. \tag{3}$$

The general form of the force–momentum balance equation can be expressed as

$$\rho\left[\frac{\partial V}{\partial t} + (\overline{V}\cdot\nabla)\overline{V}\right] = -\nabla P + F_B + \mu\nabla^2\overline{V}. \tag{4}$$

Because the flow rate is very small, the convective term in the equation can be neglected to obtain

$$\frac{dp_l}{dx} + \rho_l g\sin\beta + F_v = 0, \tag{5}$$

where β is the angle between the gravitational vector and a line normal to the grooved surface.

The primary concern of the current work to which Eq. (5) applies is to find out the dryout point, not necessarily the velocity components of liquid flow. Thus the viscous term in this expression, F_v, is substituted for $\mu\nabla^2 V$ and can be related to the fanning friction factor. Since the vapor pressure is assumed to be constant, the liquid pressure gradient can be expressed in terms of the radius of curvature as

$$\frac{dP_l}{dx} = -\frac{d}{dx}(P_v - P_l) = -\frac{d}{dx}\left(\frac{\sigma}{r(x)}\right). \tag{6}$$

Following the procedure originally outlined in [14], the form of Eq. (5) can be modified to obtain Eq. (7), with the geometric parameter defined in Eq. (8):

$$\frac{d}{dx}\left(\frac{\sigma}{r(x)}\right) = \left(\frac{2K\mu_l}{c_3 r(x)^4}\right)\Gamma_c + \rho_l g\sin\beta, \tag{7}$$

$$c_3 = 4\tan^2\alpha\left(\frac{1}{\tan\alpha} + \alpha - \pi/2\right)^3. \tag{8}$$

In the above expression, Γ_c, is the mass flow rate through the cross-section of the groove, and the parameter 'K' was originally determined in [22] as a function of the groove half angle, α, and the liquid contact angle. Eq. (8) is valid for both the evaporative and adiabatic regions.

4.1. Evaporative region

If the liquid in the evaporating region is assumed to be saturated and the heat flux along the x-direction is given by $q''(x)$, the mass flow rate at a certain position x can be expressed as

$$\Gamma_c = \int_0^{\Gamma_c} d\Gamma_c = \left(\frac{2\omega_b}{h_{fg}}\right)\int_x^{x_{max}} q''(x)\,dx. \tag{9}$$

This is for the case of a varying heat flux. The value x_{max} in Eq. (9) is the point farthest from the liquid pool at which the intrinsic meniscus could still be considered to exist. The mass flow rate is zero at the dryout point as shown in Fig. 2, and is measured from the junction between the heated and adiabatic regions of the plate. While it has been assumed in [17] that the evaporative heat flux is independent of position, a more realistic approach (used in the present study) would be to consider the axial variation in the net evaporative heat flux. Hence recourse to numerical integration and iterative techniques are needed to solve the nonlinear coupled differential equations. For the case of small inclinations, the basic governing equation was considered a weakly disturbed example of the situation with no inclination, making it suitable for solution using the perturbation technique [17].

Combining Eqs. (7)–(9), and non-dimensionalizing, the following equation is obtained:

$$\frac{dR}{dX} = -\frac{A}{R^2}\int_X^{X_{max}} Q''(X)\,dX - BR^2. \tag{10}$$

The non-dimensionalized variables and the constants, namely, A, B and r_o (reference radius of curvature) are defined as follows:

$$A = \frac{4K\nu_l\omega_b L^2 q_b}{c_3\sigma h_{fg} r_o^3}, \quad B = \frac{\rho_l g\sin\beta L r_o}{\sigma}, \quad r_o = \frac{\omega}{\cos\alpha}, \tag{11}$$

$$R(X) = \frac{r(x)}{r_o}, \quad X = \frac{x}{L}, \quad Q''(X) = \frac{q''(x)}{q_b}. \tag{12}$$

The value of the reference radius of curvature r_o for the grooves used in this study is 1.24×10^{-4} m. This is solved numerically by the fourth-order Runge–Kutta technique with the following boundary conditions (r_j is the radius of curvature at the junction of the evaporative and adiabatic sections):

$$X = 0, \quad R = \frac{r_j}{r_o}, \qquad X = X_{max}, \quad R = 0. \tag{13}$$

5. Adiabatic region

In the adiabatic region, the axial mass flow rate across any section is constant and equal to the total mass flow rate evaporated over the entire length of the evaporating region. The mass flow rate per cross-section in the x-direction, Γ_c in the adiabatic region is expressed as a function of x_{max} as follows:

$$\Gamma_c = \Gamma_j = \Gamma_o = \frac{2\omega_b}{h_{fg}} x_{max} \int_0^{x_{max}} q''(x)\,dx. \tag{14}$$

Therefore the final non-dimensionalised governing equation for the adiabatic region, is

$$\frac{dR}{dX'} = -\frac{A}{R^2} \int_0^{X'_{max}} Q''(X')\,dX' - BR^2. \tag{15}$$

This is solved by the fourth-order Runge–Kutta numerical technique, with an initially assumed value of X'_{max} using the following boundary conditions:

$$X' = L_{ad,nd}, \quad R = \frac{r_j}{r_o}, \qquad X' = 0, \quad R = 1, \tag{16}$$

where $L_{ad,nd}$ is the length of the adiabatic region, non-dimensionalized with the total channel length. An estimate of $L_{ad,nd}$ can be had from the experimental temperature profiles. For the sake of completeness in modeling the evaporation, the convective heat losses are also taken into account, in calculating the evaporative heat flux from any section of the substrate.

6. Numerical solution

The evaporative heat flux distribution is determined in numerous small sections of the substrate using the experimentally obtained temperature profile in the following way. From the experimentally measured temperature profile, the convective heat transfer coefficients of all the four sides of the substrate and the corresponding convective heat losses are evaluated using standard relations [23] as functions of position. The conduction heat rate in the solid is also evaluated from the known temperature profile. The substrate is divided into 50 small sections each with a length equal to 4×10^{-4} m. For each section, from the known value of the heat entering, the convective losses and the heat leaving by conduction are subtracted to obtain the evaporative heat flux from that section for each of the experiments reported in this work. For example, for the case of the substrate inclined at an angle of 38.66° and with a heat input of 1.71 W, the convective heat loss from the upper surface is 58 W/m^2, whereas the evaporative heat flux (the heat sink capacity of the system) is 5.6×10^3 W/m^2 at a location of 1.25 cm (the midpoint of the substrate) from the hot end. The evaporative heat flux distribution thus obtained is used subsequently to solve the model equations.

An initial value of X_{max} is assumed. The governing differential equation in the adiabatic section is solved, using the fourth-order Runge–Kutta technique, to determine the radius of curvature at the junction (r_j) of the adiabatic and the evaporative sections. This is used to solve the governing equation in the evaporative region, and the value of X_{max}, i.e. the dryout point is ascertained. If the calculated value of X_{max} is not comparable with the assumed value, under the tolerance limit specified (0.001), another iteration is performed. The assumed step sizes in the adiabatic and evaporative sections are re-checked, by comparing the values of the dryout point obtained with lower step sizes. A step size of 10^{-3} was used in both the adiabatic and evaporative sections. It is to be noted that the variation of the physical properties viz. surface tension, density, viscosity, heat of vaporization with temperature, has been incorporated in the numerical scheme for the solution of the governing equations of the evaporative and adiabatic sections.

7. Comparison between theory and experiments

The results of the numerical solution of the governing equations are presented in Table 1. For each power input, the dryout point locations, as obtained from the experiments and predicted from the numerical solution of the model equations, are presented as a function of the inclination angles. As is evident from the table, good agreement is obtained between the predicted values and the experimental results. The position of the dryout point moves closer to the cold end, with increase in inclination (opposing body force) for a particular heat input. The radius of curvature plays a critical role in the performance of microgrooved cooling devices. It not only gives a qualitative idea of the capillary pumping capacity, i.e. the capacity of the device to replenish liquid evaporated at the hotter end of the device, it can also be used to predict the operating limit [18]. From the classical Young–Laplace equation, one can envisage that the value of the curvature $(1/R)$ should be monotonically

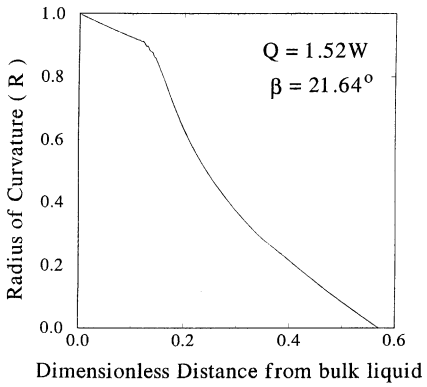

Fig. 7. Axial variation of the radius of curvature denoting dryout at 8.2 mm. Q (heat input) = 1.52 W, β (inclination) = 21.64°, T_{ref} (reference ambient temperature) = 35 °C.

decreasing from the cold to the hot end to maintain a continuous supply of liquid to the hot spot. The system will reach its capillary limit when the rate of evaporation from the film cannot be sustained by capillary pumping. At this condition, the radius of curvature will approach a value close to zero and will result in the formation of a hot spot. The variation of the dimensionless radius of curvature as a function of the dimensionless distance from the bulk liquid is plotted in Fig. 7 for the case of Q (input power) = 1.52 W and for an angle of inclination of 21.64°. It is clear from the figure that R starts with a value equal to 1.0 at the beginning of the condenser region (just before the location of the bulk pool of liquid) and the dryout location would be at a non-dimensionalized axial distance of 0.59 from the bulk liquid. This corresponds to a distance of $X_{max} = 8.2$ mm from the hot end of the substrate, whereas the experimentally obtained value is found to be 7.5 mm. Thus the present study provides a close correlation between the experimental observations and theoretical predictions and provides fundamental understanding to the problem of the formation and propagation of axial dryout points for fluid flow and evaporation from microgrooved surfaces.

8. Conclusion

Experiments are carried out in a specially designed cell to study the onset and propagation of dryout point for fluid flow and evaporation on a microgrooved silicon surface with pentane as the coolant liquid. Chemical machining method is successfully used to fabricate V-shaped axial microgrooves on a silicon substrate. Controlled heat is supplied to the top of the substrate and axial temperature distribution is accurately measured as a function of input heat and inclination of the substrate to the horizontal. The comparison between the dry (without liquid) and wet (with liquid) temperature profiles is used to verify the microcooling concept and to locate the dryout point and its propagation as a function of inclination angle and supplied heat flux. In the theoretical analysis the nonlinear governing equations for the axial flow of an evaporating thin film are solved numerically to predict the onset and location of the dryout point from a consideration of the value of the radius of curvature. The predictions from the theoretical analysis are successfully compared with the experimental results, confirming the propagation of the dry region away from the heater with increase in inclination (opposing body force) and heat input to the system.

Acknowledgements

This work is partially supported by a grant from the Department of Science and Technology, Government of India under the scheme no. SR/OY/E-13/94. Any opinions, findings and conclusions or recommendations expressed in this paper are those of the authors and do not necessarily reflect the views of the DST. The use of facilities of the Microelectronics Centre of the Electronics and Electrical Communication Engineering Department of IIT Kharagpur is gratefully acknowledged.

References

[1] T.P. Cotter, Principles and prospects of microheat pipes, in: Proceedings of the 5th International Heat Pipe Conference, Tsukuba, Japan, 1984, pp. 328–335.
[2] L.W. Swanson, G.C. Herdt, Model of the evaporating meniscus in a capillary tube, ASME J. Heat Transfer 114 (1992) 431–441.
[3] B.V. Derjagin, N.V. Churaev, The definition of disjoining pressure and its importance in the equilibrium and flow of thin films, Colloid J., USSR 38 (1976) 438–448.
[4] B.V. Derjagin, S.V. Nerpin, N.V. Churaev, Effects of film transfer upon evaporation of liquid from capillaries, Bull. Relm 29 (1965) 93–98.
[5] M.M. Weislogel, S. Lichter, Capillary flow in an interior corner, J. Fluid Mech. 373 (1998) 349–378.
[6] P.C. Wayner Jr., Y.K. Kao, L.V. LaCroix, The interline heat transfer coefficient of an evaporating wetting film, Int. J. Heat Mass Transfer 19 (1976) 487–492.
[7] F.J. Renk, P.C. Wayner Jr., An evaporating ethanol meniscus: Part II: analytical studies, J. Heat Transfer 101 (1979) 59–62.
[8] J.G. Truong, P.C. Wayner Jr., Effects of capillary and Van der Waals dispersion forces on the equilibrium profile of a wetting liquid: theory and experiment, J. Chem. Phys. 87 (1987) 4180–4188.
[9] P.C. Wayner Jr., The Effect of interfacial mass transport on flow in thin liquid films, Colloids Surf. 52 (1991) 7184.
[10] S. DasGupta, J.A. Schonberg, P.C. Wayner Jr., Investigation of an evaporative extended meniscus based on the

augmented Young–Laplace equation, J. Heat Transfer 115 (1993) 201–208.
[11] S. DasGupta, I.Y. Kim, P.C. Wayner Jr., Use of the Kelvin–Clapeyron equation to model an evaporating curved microfilm, J. Heat Transfer 116 (4) (1994) 1007–1015.
[12] B.R. Babin, G.P. Peterson, D. Wu, Steady state modelling and testing of a microheat pipe, J. Heat transfer 112 (1992) 595–601.
[13] D. Wu, G.P. Peterson, Investigation of the transient characteristics of a micro heat pipe, J. Thermophys. 5 (1991) 129–134.
[14] X. Xu, V.P. Carey, Evaporation from microgrooved surface – an approximate heat transfer model and its comparison with experimental data, J. Thermophys. 4 (1990) 512–520.
[15] G.P. Peterson, H.B. Ma, Theoretical analysis of the maximum heat transport in triangular grooves: a study of idealized micro heat pipes, J. Heat Transfer 118 (1996) 731–739.
[16] H.B. Ma, G.P. Peterson, Experimental investigation of the maximum heat transport in triangular grooves, J. Heat Transfer 118 (1996) 740–746.
[17] J.M. Ha, G.P. Peterson, Analytical prediction of axial dry out point for evaporating liquids in axial microgrooves, J. Heat Transfer 120 (1998) 453–457.
[18] R.K. Madhira, S. DasGupta, Modeling of evaporation from V-shaped microgrooves, Chem. Eng. Commun. 160 (1997) 1–24.
[19] D. Khrustalev, A. Faghri, Thermal analysis of a micro heat pipe, J. Heat Transfer 116 (1) (1994) 189–198.
[20] A. Faghri, in: Heat pipe Science and Technology, Taylor and Francis, Washington, DC, 1995, p. 625.
[21] P.C. Stephen, C.A. Busse, Analysis of heat transfer coefficient of grooved heat pipe evaporator walls, Int. J. Heat Mass Transfer 35 (2) (1992) 383–391.
[22] P.S. Ayyaswamy, I. Catton, D.K. Edwards, Capillary flow in triangular grooves, J. Appl. Mech. 41 (1972) 332–336.
[23] J.P. Holman, in: Heat Transfer, seventh ed., McGraw-Hill, London, 1992, p. 354.